ORIGINAL ARTICLE

An Effective Method Employing Alginate-TiO_2 Nanoparticles for Removing Bentazone Herbicide Residues from Water

K. Rama Raju[1], Tentu Nageswara Rao[2,3], P. Udayprakash[1], Y. Prashanthi[1]

[1]Department of Chemistry, Mahatma Gandhi University, Nalgonda, Telangana, India, [2]Department of Analytical Chemistry, Harmoni Analyticals Pvt. Ltd., IDA Jeedimetla, Hyderabad, Telangana, India, [3]Department of Chemistry, KrishnaUniversity, Machilipatnam, Andhra Pradesh, India

Abstract

Our study explored the use of alginate-TiO_2 nanoparticles to effectively remove pesticide residues from water. We synthesized alginate-TiO_2 nanoparticles and characterized them using XRD, SEM, EDS, TEM, and FTIR. We then evaluated their ability to degrade four common bentazone residues in aqueous solutions under various sunlight conditions. Sterile buffer water solutions (pH 4, 7, and 9) containing 1 mg/L bentazone were prepared in a single replicate and stored in clear glass bottles. The bottles were sealed, covered with aluminum foil, and kept in direct sunlight. At periodically, the samples were tested for bentazone concentration using a validated HPLC method. On day 10, the photolysis test showed that 4.21%, 6.83%, and 15.28% of the bentazone had been hydrolyzed in the pH-4, pH-7, and pH-9 buffers, respectively. On day 2, the photocatalysis test using nanocatalyst revealed that 89.20%, 90.26%, and 97.12% of the bentazone were catalyzed, respectively. According to the findings, nanocatalyst is an effective decontaminating agent for removing pesticide residues from water. Alginate-TiO_2 nanocatalyst gives cost-effective, efficient, and environmentally friendly alternatives to traditional decontamination methods. Our study suggests that alginate-TiO_2 nanocatalyst is a promising nanomaterial for removing pesticide residues from water, with potential applications in wastewater treatment and environmental remediation. We hope that our findings will encourage further research on this issue and contribute to the development of sustainable and environmentally friendly solutions for enhancing water quality.

Key words: Alginate-TiO_2 nanocatalyst, pesticide residues, HPLC, photocatalysis, photolysis

INTRODUCTION

Pesticide residues are the traces of pesticides that may remain on or in food after being applied during agricultural processes. Consumers, farmers, and environmentalists may all be concerned about these residues, which have the potential to harm human health and the environment. The World Health Organization (WHO) and other regulatory bodies worldwide have set maximum residue limits (MRLs) to ensure food safety. Pesticides are essential for protecting crops from a wide range of pests, including insects, weeds, and fungi. They also play an important role in increasing agricultural yields, which is critical for countries facing food shortages.

The WHO actively reviews evidence and develops internationally accepted MRLs to protect consumers from pesticides' harmful effects.[1] It is important to note that none of the pesticides approved for use on food in international trade are genotoxic, which means they do not damage DNA, cause mutations, or cause cancer.[2] Pesticides cause adverse effects only at specific levels of exposure.[3] Nonetheless, pesticide residues are one of the leading causes of death by self-poisoning, especially in low- and middle-income countries, emphasizing the need for strict regulation and control over their production, distribution, and use.[4]

Regular monitoring of residues in food and the environment is required to protect public health. The long half-life of some

Address for correspondence:
Dr. Y. Prashanthi, Department of Chemistry, Mahatma Gandhi University, Nalgonda, Telangana, India. Mobile: 9010203857.
E-mail: dryprasanthi@gmail.com

Received: 12-07-2024
Revised: 16-09-2024
Accepted: 25-09-2024

pesticides, such as DDT, in soil and water presents ongoing challenges.[5] Although persistent organic pollutants have been banned by international treaties such as the Stockholm Convention of 2001, their legacy remains a source of concern due to their ability to persist in the environment for years and accumulate in the food chain.[6,7] Finally, while pesticides are necessary for modern agriculture, their residues must not endanger human health or the environment.[8,9] This balance is maintained through stringent regulation, continuous monitoring, and adherence to established safety standards. Consumers can also play a role by learning about the origins of their food and the practices used to produce it.[10,11]

Bentazone, a selective post-emergence herbicide, inhibits photosynthesis in target plants.[12] It binds specifically to a protein in photosystem II, which is an essential component of the photosynthetic pathway.[13] This binding disrupts the normal flow of electrons through the photosystem, preventing light energy from being converted into chemical energy and eventually causing the plant to die.[14] Bentazone is effective against a wide range of broadleaf weeds and yellow nutsedge, and it is commonly used in soybeans, corn, and rice. Its selectivity is due to the ability of certain crops to metabolize the herbicide without harm.[15] However, its application necessitates careful management to avoid potential environmental consequences, such as leaching into groundwater and the development of resistant weed species.[16]

Nanocatalysts are nanoscale materials that accelerate chemical reactions. They have numerous applications, including energy conversion, environmental remediation, and biomedical engineering.[17] One of the most promising applications of nanocatalysts is the removal of antibiotic residues from water. Antibiotic residues are the traces of antibiotics found in water after they have been used in human and animal health care, agriculture, and aquaculture.[18] They endanger the environment and public health by encouraging the growth of antibiotic-resistant bacteria and upsetting the natural balance. To degrade antibiotic residues in water, various methods can be used, including photocatalysis, electrocatalysis, the Fenton reaction, and advanced oxidation. These mechanisms involve the generation of reactive oxygen species such as hydroxyl radicals, superoxide radicals, and hydrogen peroxide, which can oxidize and degrade antibiotic molecules.[18] Adsorption of pesticide residues on the surface of nanocatalysts reduces their concentration and mobility in water. Nanocatalysts have several advantages over traditional methods of removing antibiotic residues from water, including high efficiency, low cost, ease of synthesis, and recyclability. However, some issues and limitations need to be addressed, such as the stability, toxicity, and recovery of nanocatalysts in water systems.[19]

Photolysis and photocatalysis are two processes in which light interacts with matter. Photolysis is the process of breaking chemical bonds with light, whereas photocatalysis is the use of light to accelerate a chemical reaction in the presence of a photocatalyst.[20] A photocatalyst is a material that absorbs light and produces excited states that can interact with other molecules.[21] Photocatalysis can be used in a variety of environmental applications, including the removal of organic pollutants, the production of hydrogen through water splitting, and the reduction of carbon dioxide. Photocatalysis can use solar or visible light, making it a green and sustainable technology.[22]

Alginate-titanium dioxide (TiO_2) nanocomposites are an intriguing field of research, combining the biocompatibility and natural origin of alginate with the photocatalytic properties of TiO_2.[23] These materials have been investigated for a wide range of applications, including biomedical engineering and environmental remediation. TiO_2-modified alginate fibers can create antibacterial dressings, particularly in healthcare settings.[24] The incorporation of TiO_2 into alginate matrices has been explored for the degradation of pollutants, such as the catalytic hydrogenation of nitrophenols to aminophenols. This demonstrates the environmental applications of these composites.[25] The food industry now uses sodium alginate/TiO_2 nanocomposite films with antimicrobial properties for packaging and preservation. The ability to add other nanoparticles, such as silver, to enhance the functional properties of these nanocomposites increases their versatility. Consider hybrid Alginate/TiO_2/Ag bio-nanocomposite beads. Research continues to broaden the capabilities of these materials, discovering their full potential in various fields.[26]

This study used alginate-TiO_2 nanoparticles as photocatalysts to breakdown bentazone in water samples. The results demonstrated the high efficacy of this method in mineralizing and removing bentazone, leaving only harmless byproducts such as carbon dioxide and water.

EXPERIMENTAL

Synthesis of alginate-TiO_2 nanoparticles

Preparation of 10% alginate solution

To prepare a stock solution, dissolve 10 g of alginate powder in 100 mL of distilled water.

Synthesis of TiO_2 nanoparticles

The TiO_2 nanoparticles were prepared by dropping 4 mL of titaniumtetrachloride (TiCl4) into 100 mL of distilled water containing 1% hydrochloric acid (HCl) at 5°C, ultrasonically for 1 h at 80°C, and kept for 16 h at 80°C in a thermostat-controlled oven.

$TiCl_4+2H_2O$ yields TiO_2+4HCl.

The white precipitate was washed 8 times in distilled water using a refrigerated centrifuge before being washed with methanol. The methanol was decanted, and the precipitate (TiO_2 nanoparticles) was dried at 80°C for 4 h.

Synthesis of alginate-titanium dioxide (TiO_2)

Mixing

The alginate solution is infused with the TiO_2 nanoparticle suspension. The mixture is Crosslinking: The alginate solution containing dispersed TiO_2 nanoparticles is added dropwise into the 0.5% $CaCl_2$ solution. This can be done using a syringe to form uniform beads.[27] The beads are left in the $CaCl_2$ solution for a specific period to ensure complete crosslinking. This duration can vary but is typically around 1 h.

Washing

The formed beads are collected and washed thoroughly with distilled water to remove any unreacted calcium ions and other impurities.

Drying

The final alginate-TiO_2 nanocomposite beads are obtained by drying them at 40° in an oven.

Characterization of alginate-TiO_2 nanoparticles

The synthesized nanoparticles were characterized using a variety of techniques, including X-ray diffraction (Rigaku Smartlab SE Multipurpose XRD) to determine phase composition, lattice parameters, and crystallite size. The elemental composition and purity of the products were determined using energy dispersive X-ray spectroscopy (Malvern-EDX). The functional groups and bonds found in the precursors and products are identified using Fourier transform infrared spectroscopy (Agilent 4300-FTIR). Scanning electron microscopy (Tescan-SEM) can examine Alginate-TiO_2 nanoparticles' morphology, size, shape, and distribution. Transmission electron microscopy (Tescan-TEM) measures the size, shape, and crystal structure of Alginate-TiO_2 nanoparticles. Thermogravimetric analysis (TA Instruments-TGA) can determine the thermal stability, decomposition, and phase transitions of Alginate-TiO_2 nanoparticles.

Preparation and sterilization of buffer solutions

The buffer was used at a concentration of 0.01 M to reduce any potential catalytic effects. The pH, concentration, preparation date, expiration date, and study number were all marked on the labels of the buffer solutions. Following preparation, a 0.45 µm filter was used to sterilize the buffer solutions.

Strile pH 4 buffer

A 0.01 M acetic acid solution was prepared by adding 0.58 mL of glacial acetic acid to a 1000 mL volumetric flask and diluted to volume with distilled water.

A 0.01 M sodium acetate solution was prepared by adding 0.8276 g sodium acetate to a 1000 mL volumetric flask and diluting to volume with distilled water.

820 mL of 0.01 M acetic acid solution and 180 mL of 0.01 M sodium acetate solution were combined to create the 0.01 M pH 4 buffer solution. Finally, a 50% (w/w) sodium hydroxide solution was used to adjust the pH. After the buffer solution's pH of 4.01 was confirmed, it was filtered through a 0.45 µm membrane filter.

Strile pH 7 buffer

About 3.1204 g of sodium phosphate monobasic (dihydrate) were added to a 1000 mL volumetric flask, and the mixture was diluted to volume with distilled water to create a 0.02 M sodium phosphate monobasic solution.

About 2.8512 g of sodium phosphate dibasic (anhydrous) were added to a 1000 mL volumetric flask, and the mixture was diluted to volume with distilled water to create a 0.02 M sodium phosphate dibasic solution.

A 1000 mL volumetric flask was filled with roughly 195 mL of 0.02 M sodium phosphate (monobasic) and 304 mL of 0.02 M sodium phosphate (dibasic) to create the 0.01 M pH 7 buffer solution. Water was added to the contents to create a 0.01 M pH 7.0 phosphate buffer solution. Salt hydroxide solution containing 50% (w/w) was used to make the final pH adjustments. After the buffer solution's pH of 7.01 was confirmed, it was filtered through a 0.45 µm membrane filter.

Strile pH 9 buffer

1.54532 g of boric acid were transferred to a 50 mL volumetric flask and diluted to volume with distilled water to create a 0.5 M boric acid solution. The 0.5 M boric acid solution was divided into 20 mL aliquots, which were then transferred to a 1000 mL volumetric flask and diluted to volume with distilled water. A 0.01 M, pH 9.0 borate buffer solution was created by adjusting the 0.01 M boric acid solution to a pH of 9 using 50% (w/w) sodium hydroxide solution. After the buffer solution's pH (9.03) was confirmed, it was filtered through a 0.45 µm membrane filter.

Sterility measurements

During the study, the pH 9 buffer test system's sterility was checked. To assess sterility, agar plates were utilized. One milliliter of the test solution was aseptically added to a plate for sampling. For 2 days, the plates were incubated at 35 ± 2C in an incubator. Following incubation, the Agar plates were inspected to look for signs of microbial growth (Bacteria) in comparison to the control Agar plate; none was found.

HPLC chromatographic conditions

A Shimadzu high-performance liquid chromatography instrument with an Agilent C18 (250 mm × 4.6 mm × 5 µm) column and a 220 nm PDA detector was used to analyze the sample. 1.0 ml/min was the flow rate, and the injection volume was 10 µL. To avoid contamination, acetonitrile was used to rinse the column following each run. The analyte was retained for 4.2 min during the 10 min run time. The gradient of A - Acetonitrile 70% and B - 0.1% OPA in 30% HPLC water made up the mobile phase.

Method validation

Method specificity

Untreated control samples of pH 4, 7 and 9 sterile buffer solutions, methanol and distilled water were assayed for method specificity.

Linearity of response

A stock solution of bentazone standard was prepared by weighing 10.15 mg of 99.5% purity reference standard into a 10 mL volumetric flask and brought to volume with methanol. A series of calibration solutions were then prepared by diluting the appropriate volume of stock solution into different 10 mL volumetric flasks and bringing to volume with acetonitrile. The prepared calibration solutions 0.01 µg/mL (L1), 0.1 µg/mL (L2), 0.5 µg/mL (L3), 1.0 µg/mL (L4), 2.0 µg/mL (L5), and 5 µg/mL (L6) were analyzed by high pressure liquid chromatography. A linear curve was plotted for the concentration of standard versus observed peak area and the correlation coefficient was determined.

Assay accuracy and precision

Validation includes the analysis of fortified samples and an untreated (blank) sample. Fortified samples were prepared by adding a known quantity of bentazoneto distilled water followed by sample work up. The quantity of bentazonein the distilled water was then determined by HPLC method. The fortified samples were at 1 × LOQ level = 0.01 µg/mL and 10 × LOQ = 0.1 µg/mL concentration level. Method validation consisted of five replicates at each fortification level. The percentage recovery and % relative standard deviation was calculated from the response area of fortified samples.

Limit of quantification (LOQ)

The lowest validated level with sufficient recovery is defined as the LOQ. The LOQ was determined using 5 injections of 0.01 µg/mL fortification level recovery samples. Low level recovery solutions were used for LOQ.

Photolytic and photocatalytic studies

A 1 mg L-1 concentration of bentazone was spiked to study the photocatalysis of bentazone residues in water. Aqueous buffer solutions with pH values of 4.0, 7.0, and 9.0 were used for the experiment. Single replications were carried out at each fortification level in addition to control samples for comparison. Two sets of spiked concentrations are prepared for the studies. One set of samples received the catalyst (Alginate-TiO_2NPs), while the other set of samples was examined without the catalyst. The samples were exposed to the sun directly. Aliquots of the sample were taken at prearranged intervals. Water samples were collected over the period, and their temperatures varied from 25 to 43°C.A 0.2 m PTFE membrane filter was used to filter the samples that were collected during different sampling occasions. The filtrates were then collected in vials with an amber color. Prior to HPLC-PDA analysis, each sample was kept at 5°C in the dark. A Beckman cooling centrifuge operating at 3000 rotations per minute was used to centrifuge the samples fortified with Alginate-TiO_2NPs for five minutes at 5°C. The supernatants were moved to amber-colored bottles and kept in the dark at 5°C until analysis to prevent further degradation of residues.

RESULTS AND DISCUSSION

Characterization of alginate-TiO_2 nanoparticles

FTIR analysis

The FTIR spectra of the samples used to examine the quality and synthesis of alginate-TiO_2 nanoparticles are displayed in Figure 1. O-H stretching (3200–3450 cm^{-1}), C=O stretching (1600–1700 cm^{-1}), and C-O-C stretching (1000-1200 cm^{-1}) are three of alginate's distinctive peaks. Between 400 and 800 cm^{-3}, TiO_2 peaks usually show up, indicating Ti-O and Ti-O-Ti stretching vibrations. The FTIR spectrum [Figure 1] exhibits shifts in its characteristic peaks when alginate interacts with TiO_2, indicating bond formation or interaction between the two components.[28] Alginate and TiO_2 peaks can

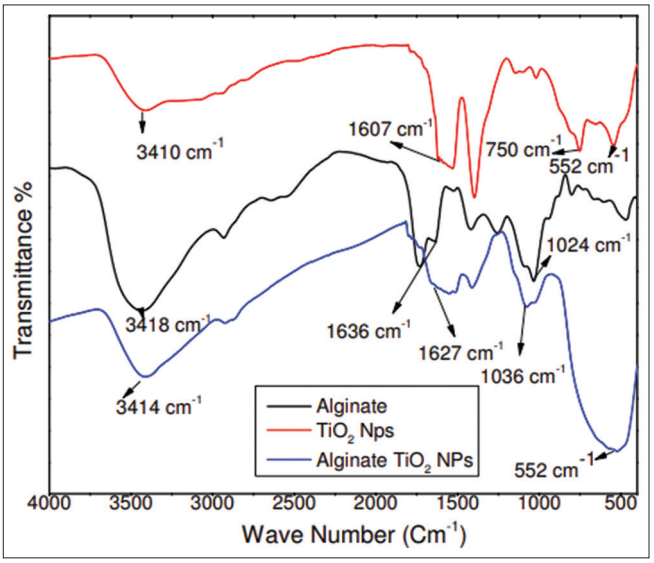

Figure 1: FTIR spectra of alginate, TiO_2 NPs and alginate-TiO_2 NPs

be seen in the FTIR spectrum, indicating that the synthesis of alginate-TiO_2 nanoparticles was successful.

XRD analysis

Figure 2 shows the XRD patterns of the nanoparticles. Alginate's diffraction pattern is devoid of crystalline phases. Nevertheless, at 2θ=13.85°, alginate displays a broad and feeble diffraction peak. It might have happened because of an instrumental mistake. Consequently, it generally refers to the non-crystalline, amorphous structure of alginate. TiO2's rutile crystalline structure was confirmed by its maximum intense peak at 31.81°. The diffraction angles that are corresponded to the Miller indices (hkl) (110), (101), (200), (211), (220), (002), (310), and (301) are 36.19°, 40.12°, 45.37°, 56.60°, 62.92°, 64.28°, 69.76°, and 70.04°, respectively.[29]

TGA analysis

The TGA curve of alginate-TiO_2 nanoparticles is shown in Figure 3. The curve represents three major mass reduction steps.

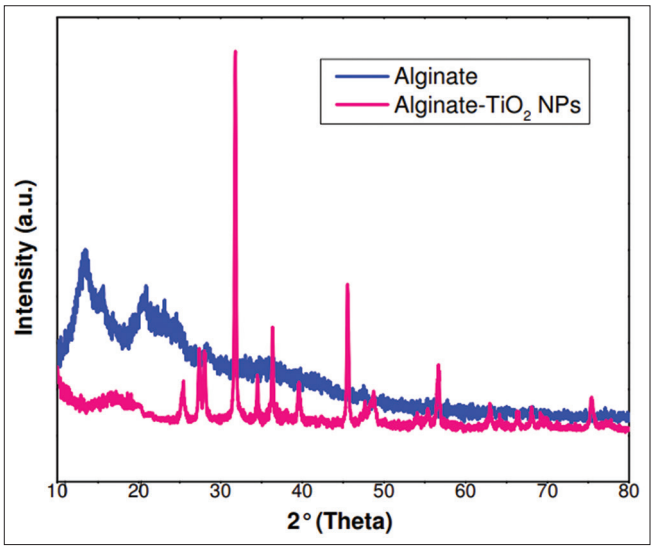

Figure 2: XRD of alginate, and alginate-TiO_2 NPs

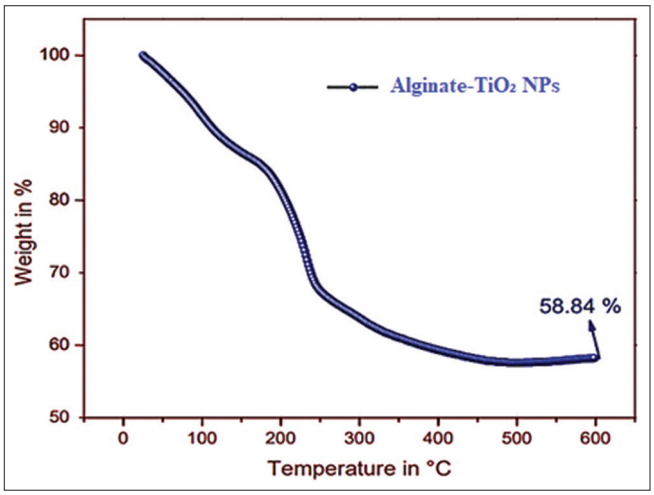

Figure 3: TGA Curve of Alginate-TiO_2 nanoparticles

The first step involves removing residual water and organic solvents from the sample at temperatures ranging from room temperature to approximately 200°C. The remaining mass in this step is around 92%. The second step, from 200°C to 600°C, is caused by the degradation of organic precursors and the formation of the titanium oxide phase. The remaining mass in this step is about 70%. At 600°C, the sample retains 59% of its initial mass, indicating a high yield of alginate-TiO_2 nanoparticles.

EDS analysis

Figure 4 represents the elemental composition of the Alginate-TiO_2 NPs was revealed by EDS analysis, as shown in Figure 4. At 2.3 keV, 1.6 keV, and 2.0 keV, respectively, three distinct peaks corresponding to carbon, oxygen, and titanium elements were observed. The weight ratio of C: O:Ti was approximately 43.11:38.82:18.08, indicating that Alginate-TiO_2 NPs were formed.

SEM analysis

As shown in Figure 5, particles in certain areas of the sample are more connected to one another, resulting in larger clusters. This implies that some of the particles in the sample act as seed particles, attracting other particles through condensation. As a result, the sample shows agglomeration

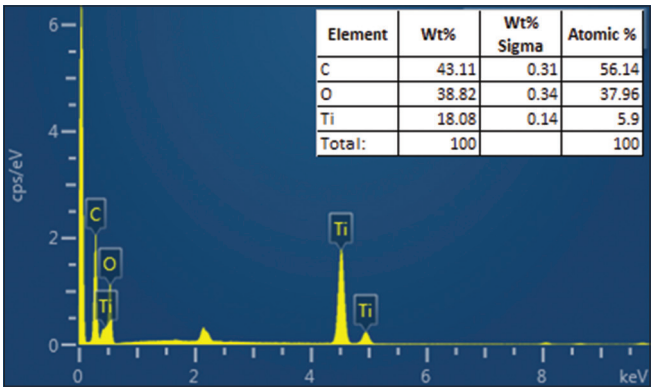

Figure 4: EDS of alginate-TiO_2 nanoparticles

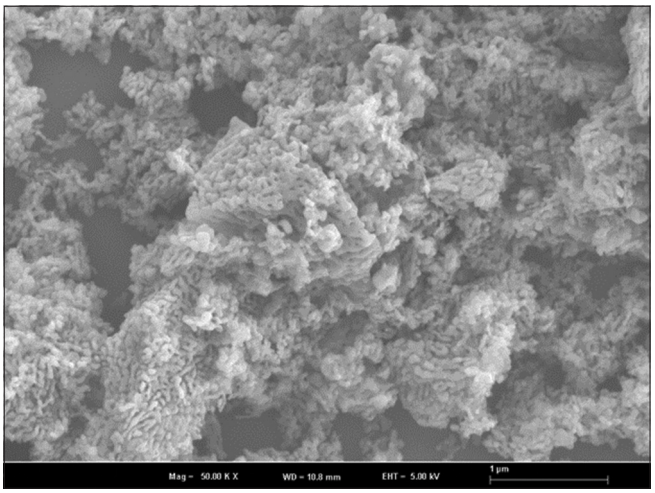

Figure 5: SEM image of alginate-TiO_2 nanoparticles

in certain areas. SEM can also show the degree to which nanoparticles aggregate. Alginate can reduce aggregation, resulting in better dispersion of the nanoparticles.

TEM analysis

Figure 6 shows a TEM image of alginate-TiO_2 nanoparticles, ranging in size from 20 to 150 nm. The sample exhibits a high degree of crystallinity, particle aggregation, and a distinct cubic structure. These characteristics indicate that alginate-TiO_2 nanoparticles have a unique structure and shape.

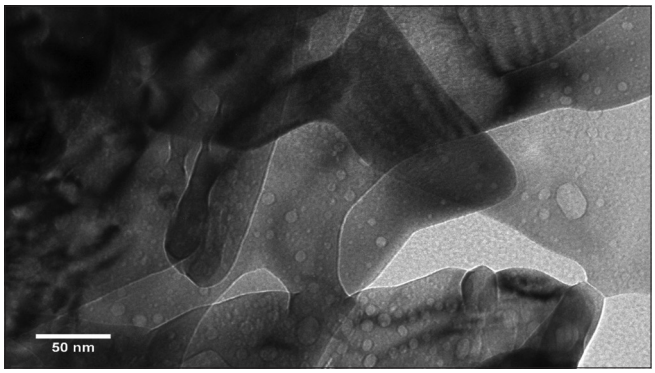

Figure 6: TEM image of alginate-TiO_2 nanoparticles

Table 1: Detector linearity test

Concentration(µg/mL	Areain (mAU)
0.01	395
0.1	2915
0.5	16002
1	31587
2	63524
5	157810
Slope	31574.14
Intercept	63.27
cc	1.0000

Method validation

Specificity

The analytical method was found to be specific. There was no interference observed at the retention time of the bentazone Technical peak. The % difference in retention time of test item and reference standard found to be within ± 5.0%.

Linearity

The analytical method was found to be linear in the range 0.01 mg/L to 5.0 µg/mL with correlation co-efficient (R^2) =1.0000, Slope = 31574.14 and Intercept = 63.27. The results of area of concentrations are presented in Table 1. The linearity curve is presented in Figure 7.

Recovery and repeatability

Multiple recovery control samples (n = 2) at each of 2 fortification levels equivalent to 0.05 mg/L and 0.5 mg/L for three buffers. Bentazonein the final solution were assayed using HPLC. The results are presented in Table 2.

Limit of Quantitation (LOQ)

LOQ was established to be 0.01 µg/mL from the lower level recovery test in sterile pH-4, pH-7 and pH-9 buffers.

Photolytic studies and photocatalytic studies

The degradation results of Bentazone in water showed the residues are highly stable, the stability decreased with

Table 2: Recovery and repeatability of bentazone in acidic, neutral and basic waters

Sample code	Recovery (%) of acidic water	Recovery (%) of neutral water	Recovery (%) of basic water
LOQ Level_R1	88.23	90.23	90.14
LOQ Level_R2	88.20	89.56	89.53
LOQ Level_R3	87.14	90.17	88.96
LOQ Level_R4	89.83	88.96	91.04
LOQ Level_R5	89.23	90.78	91.42
LOQ×10 Level_R1	90.23	92.12	90.52
LOQ×10 Level_R2	91.28	91.56	92.74
LOQ×10 Level_R3	90.56	92.79	92.41
LOQ×10 Level_R4	92.21	90.27	91.74
LOQ×10 Level_R5	91.85	90.52	92.07
Average	89.88	91.74	91.74
Standard Deviation	1.68	1.16	1.25
%RSD	1.87	1.27	1.37

Table 3: Photolysis of Bentazone under direct sunlight in acidic, neutral and basic water (without catalyst)

Occasion (Days)	Residue Level	Log	Acidic water		Residue Level	Log	Neutral water		Residue Level	Log	Basic water	
0	1.002	0.0009	Slope	−0.140	0.995	−0.0022	Slope	−0.149	0.971	−0.0128	Slope	−0.159
3	0.821	−0.0857	Half-life (DT50)	2.16	0.792	−0.1013	Half-life	2.02	0.601	−0.2211	Half-life (DT50)	1.90
5	0.612	−0.2132			0.482	−0.3170			0.296	−0.5287		
7	0.082	−1.0851			0.074	−1.1308			0.068	−1.1675		
10	BDL	BDL	Intercept	0.177	BDL	BDL	Intercept	0.171	BDL	BDL	Intercept	0.112
			CC	0.972			CC	0.987			CC	0.941

Table 4: Photocatalysis of Bentazone in presence of Alginate-TiO_z nanoparticles under direct sunlight in acidic, neutral and basic water

Occasion (hours)	Residue Level	Log	Acidic water		Residue Level	Log	Neutral water		Residue Level	Log	Basic water	
0	1.101	0.0418	Slope	−0.091	1.002	0.0009	Slope	−0.092	0.998	−0.0009	Slope	−0.099
6	0.367	−0.4353	Half-life (DT50)	3.29	0.292	−0.5346	Half-life	3.27	0.215	−0.6676	Half-life (DT50)	3.04
12	0.091	−1.0410			0.082	−1.0862			0.072	−1.1427		
18	0.026	−1.5850			0.022	−1.6576			0.015	−1.8239		
24	BDL	BDL	Intercept	0.068	BDL	BDL	Intercept	0.010	BDL	BDL	Intercept	-0.017
			CC	0.904			CC	0.912			CC	0.998

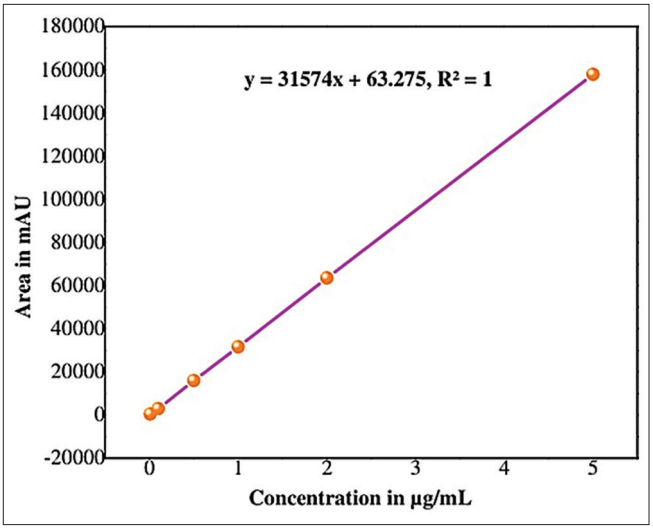

Figure 7: Linearity curve of bentazone standard

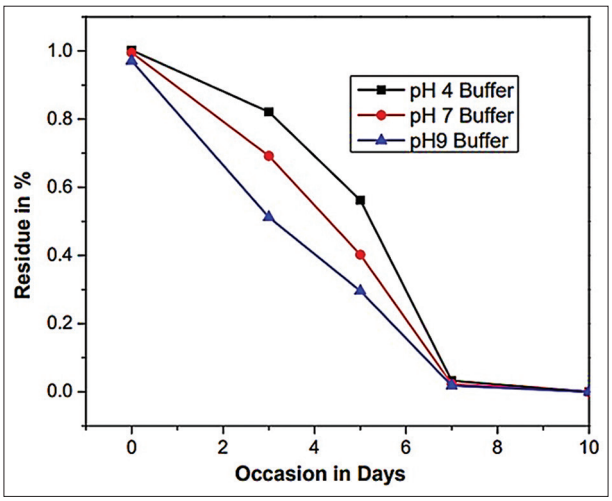

Figure 8: Photolysis curve of bentazone under direct sunlight in acidic, neutral and basic water (without catalyst)

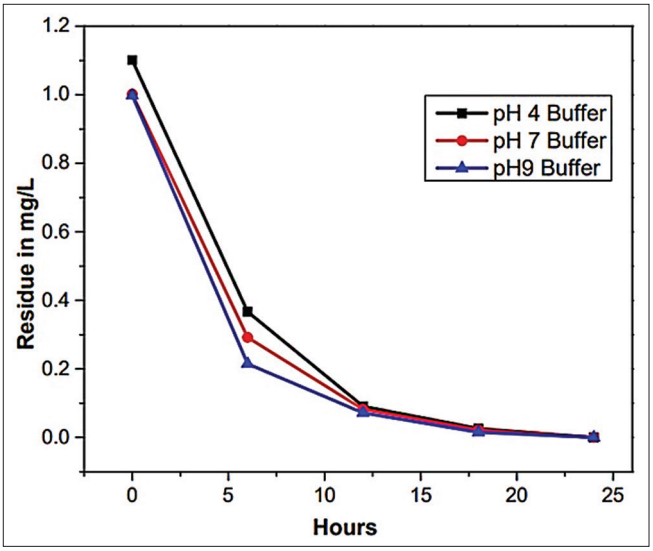

Figure 9: Photocatalysis Curve of Bentazone under direct sunlight in acidic, neutral and basic water (without catalyst)

decreasing pH. The half-life of Bentazone was 2.16, 2.02 and 1.90 days in acidic, neutral and basic pH's respectively without catalyst shown in Table 3 and Figure 8. Whereas the half-lifeof bentazonein presence of catalyst in different aqueous buffers was recorded to be 3.29 h in acidic water, 3.27 h in neutral water and 3.04 h in basic water shown in Table 4 and Figure 9.

CONCLUSIONS

This study shows that Alginate-TiO_2NPs can effectively remove pesticide residues from water, a significant environmental and public health concern. Under various conditions, the nanomaterial demonstrated excellent adsorption performance and stability, and it was easily regenerated and reused. The DT50 value, also known as the half-life, is an important parameter in environmental chemistry because it represents how long it takes for a substance's concentration to decrease to half of its initial value due to degradation. Photolytic studies involve direct light absorption, whereas photocatalytic studies use light-activated catalysts. The DT50 difference can be significant, as photocatalytic reactions are more efficient and faster due to the catalyst's ability to reduce activation energy. This efficiency is critical in environmental applications like pesticide residue degradation, where shorter reaction times can lead to more effective remediation strategies. Understanding these distinctions is critical for creating advanced materials and technologies for environmental sustainability and pollution reduction. This study suggests new applications for Alginate-TiO_2 nanoparticles in wastewater treatment and environmental remediation, and encourages further research on the topic. Using this nanomaterial, we hope to provide long-term and environmentally friendly solutions to improve water quality.

AKNOWLEDGEMENT

The authors gratefully acknowledge the Department of Chemistry at Mahatma Gandhi University, Nalgonda, for their invaluable contributions and insightful scientific discussions. Furthermore, we acknowledge the continuing backing of Harmoni AnalyticalsPvt. Ltd, IDA Jeedimetla, which has been critical to the successful completion of this project.

REFERENCES

1. Dinede G, Bihon W, Gazu L, Foukmeniok Mbokou S, Girma S, Srinivasan R, *et al*. Assessment of pesticide residues in vegetables produced in central and eastern Ethiopia. Front Sustain Food Syst 2023;7:1143753.
2. Froger C, Jolivet C, Budzinski H, Pierdet M, Caria G, Saby NP, *et al*. Pesticide residues in French soils:

Occurrence, risks, and persistence. Environ Sci Technol 2023;57:7818-27.
3. Yura WF, Muhammad FR, Mirza FF, Maurend YL, Widyantoro W, Farida SS, *et al*. Pesticide residues in food and potential risk of health problems : A systematic literature review. IOP Conf Ser Earth Environ Sci 2021;894:012025.
4. Wahab S, Muzammil K, Nasir N, Khan MS, Ahmad MF, Khalid M, *et al*. Review advancement and new trends in analysis of pesticide residues in food: A comprehensive review. Plants (Basel) 2022;11:1106.
5. Mondal P, Banga U, Vishwavidyalaya K, Ghosh SK, Chandra B, Viswavidyalaya K, *et al*. Pesticide Residues : Analysis. Impact and Mitigation. New Delhi: Association for Agriculture, Environment and Biotechnology; 2021.
6. Brinco J, Guedes P, Gomes da Silva M, Mateus EP, Ribeiro AB. Analysis of pesticide residues in soil: A review and comparison of methodologies. Microchem J 2023;195:109465.
7. Tudi M, Ruan HD, Wang L, Lyu J, Sadler R, Connell D, *et al*. Agriculture development, pesticide application and its impact on the environment. Int J Environ Res Public Health 2021;18:1-24.
8. Terfe A, Mekonen S, Jemal T. Pesticide residues and effect of household processing in commonly consumed vegetables in Jimma Zone, Southwest Ethiopia. J Environ Public Health 2023;2023:1-12.
9. Faraj TK, El-Saeid MH, Najim MM, Chieb M. The impact of pesticide residues on soil health for sustainable vegetable production in arid areas. Separations 2024;11:46.
10. Fazeli-Nasab B, Shahraki-Mojahed L, Beigomi Z, Beigomi M, Pahlavan A. Rapid detection methods of pesticides residues in vegetable foods. Chem Methodol 2022;6:24-40.
11. Zhang Y, Zheng Q, Chen X, Guan Y, Dai J, Zhang M, *et al*. Comparison and analysis of several quantitative identification models of pesticide residues based on quick detection paperboard. Processes 2023;11:1854.
12. Ali L, Jo H, Song JT, Lee JD. The prospect of bentazone-tolerant soybean for conventional cultivation. Agronomy 2020;10:1650.
13. Schuhmann A, Klammler G, Weiss S, Gans O, Fank J, Haberhauer G, *et al*. Degradation and leaching of bentazone, terbuthylazine and S-metolachlor and some of their metabolites: A long-term lysimeter experiment. Plant Soil Environ 2019;65:273-81.
14. Porini JA, Escandar GM. Spectrofluorimetric study of the herbicide bentazone in organized media: Analytical applications. Anal Methods 2011;3:1494-500.
15. Ali L, Jo H, Song JT, Lee JD. Evaluation of bentazone reaction by growth stage and bentazone dose across soybean genotypes. Plant Breed Biotechnol 2021;9:331-44.
16. Utzeri G, Guirado-Moreno JC, Cova TF, Pais AA, Batista De Carvalho LA, Ibeas S, *et al*. Reusable and effective polyacrylic membranes for mecoprop and bentazon extractions. NPJ Clean Water 2024;7:1-13.
17. Roy A, Elzaki A, Tirth V, Kajoak S, Osman H, Algahtani A, *et al*. Biological synthesis of nanocatalysts and their applications. Catalysts 2021;11:1494.
18. Somwanshi SB, Somvanshi SB, Kharat PB. Nanocatalyst: A brief review on synthesis to applications. J Phys Conf Ser 2020;1644:012046.
19. Ingle AP, Chandel AK, Philippini R, Martiniano SE, Da Silva SS. Advances in nanocatalysts mediated biodiesel production: A critical appraisal. Symmetry (Basel) 2020;12:1-21.
20. Elayaperumal M, Duraisamy M, Ganesh H. Photocatalysis: Present, Past and Future. Millersville, PA: Materials Research Forum LLC; 2018. p. 183-206.
21. Kumari H, Sonia, Suman, Ranga R, Chahal S, Devi S, *et al*. A review on photocatalysis used for wastewater treatment: Dye degradation. Water Air Soil Pollut 2023;234:349.
22. Sordello F, Calza P, Minero C, Malato S, Minella M. More than one century of history for photocatalysis, from past, present and future perspectives. Catalysts 2022;12:1572.
23. Omer RA, Abdel-Rahman HK, Saleh MM, Al-Hawezi SS, Ikram FS. Effect of adding titanium dioxide nanoparticles on anti-microbial activity and surface detail reproduction of dental alginate. J Baghdad Coll Dent 2023;35:36-48.
24. Borkowski D, Krucińska I, Draczyński Z. Preparation of nanocomposite alginate fibers modified with titanium dioxide and zinc oxide. Polymers (Basel) 2020;12:1040.
25. Zhao K, Feng L, Li Z, Fu Y, Zhang X, Wei J, *et al*. Pilm and the recovery of TiO_2 nanoparticles. RSC Adv 2014;4:51321-9.
26. Bakil SN, Abdullah HZ, Selimin MA, Lee TC, Idris MI. Bio-composite of sodium alginate-titanium dioxide for wound healing applications. Mater Sci Forum 2020;1010:555-60.
27. Ibrahim MA, Nasr GM, Ahmed RM, Kelany NA. Physical characterization, biocompatibility, and antimicrobial activity of polyvinyl alcohol/sodium alginate blend doped with TiO_2 nanoparticles for wound dressing applications. Sci Rep 2024;14:5391.
28. Fundador EO, Villanueva JM, Fundador NG, De Cadiz AE. Antimicrobial property of sodium alginate/Tio_2 nanocomposite film. Philipp J Sci 2018;147:545-50.
29. Uddin MJ, Islam JM, Rahman MA, Khan MA. Development of photoactive titanium dioxide doped sodium alginate film for dye sensitized solar cell application. Int J Thin Film Sci Technol 2017;6:135-8.

Source of Support: Nil. **Conflicts of Interest:** None declared.